IEEE Access
Multidisciplinary ⋮ Rapid Review ⋮ Open Access Journal

Received July 15, 2021, accepted July 27, 2021, date of publication July 30, 2021, date of current version August 5, 2021.

Digital Object Identifier 10.1109/ACCESS.2021.3101501

Grid-Voltage-Feedback Active Damping With Lead Compensation for LCL-Type Inverter Connected to Weak Grid

CHENGBI ZENG, HANWEN WANG, SUDAN LI, AND HONG MIAO
School of Electrical Engineering, Sichuan University, Chengdu, Sichuan 610065, China
Corresponding author: Hong Miao (miaohong@scu.edu.cn)

ABSTRACT To improve the robustness and stability of the LCL inverter connected to weak grid, this paper proposes a novel active damping based on voltage of point common coupling (v_{pcc}) feedback. A phase lead compensator is proposed in the v_{pcc} feedback loop to compensate system phase margin (PM). Theoretical analysis of the effectiveness, detailed parameter setting, stability analysis for proposed active damping adopting lead compensator, named as LC AD, are all described. Simulation and experiment results show that comparing to conventional high pass filter (HPF) AD, the proposed LC AD provides more effective damping effect for the LCL inverter adopting quasi-proportional resonant (QPR) controller under weak grid.

INDEX TERMS Weak grid, LCL filter, grid-connected inverter, active damping.

I. INTRODUCTION

The grid-connected inverter, together with a filter, plays an important role as the connection hub between distributed renewable power generations and the grid [1]–[3]. Typically, LCL filter is widely used in grid-connected inverters for its advantages of small size, relatively strong ability to suppress harmonics, etc. However, LCL resonance may cause the system to oscillate or even to lose stability without appropriate damping scheme [4], [5]. On the other hand, with the penetration increasing of distributed generation (DG), the grid impedance cannot be ignored anymore and the grid presents the characteristics of weak grid instead of conventional ideal grid [6], [7]. The presence of grid impedance will cause the resonance frequency of LCL inverter system to fluctuate, which may decrease system stability margin and imposes more critical requirements on the system damping scheme [8].

Presently, damping methods of LCL filters can be classified into passive damping (PD) and active damping (AD) [9]. PD has an excellent damping effect, but a relatively large loss is introduced due to the adopted resistor [10]. AD adopts the method of reconstructing system transfer function to avoid resonance and it includes methods such as resonance peak compensation, system order reduction and state variable feedback, etc. The compensation method is usually implemented by cascading a notch filter with the current regulator to compensate the LCL resonant peak [11], where the notch frequency should be aligned exactly to the resonant frequency of the LCL filter [12]. However, parameter variations of the LCL filter and the presence of weak grid impedance will cause resonance frequency to fluctuate, which will deteriorate the original damping effect or even make the compensation damping scheme futile [13]. The reduction of system order can be achieved by employing methods such as splitting-capacitor strategy [14] and the weighted current method [15]. However, the robustness of the system is poor due to their high dependence on the filter parameters and the presence of grid impedance under weak grid may result in the failure of the system order reduction.

The fundamental principle of state variable feedback AD is to introduce a virtual resistor to the LCL system to consume oscillation power. This type AD usually adopts capacitor current feedback (CCF), capacitor voltage feedback (CVF) and multi state variable feedback (MSVF) [16]–[20], etc. CCF constructs a virtual resistor in parallel with the filter capacitor [16], which is simple and can effectively suppress the LCL resonance [17]. CVF is also called HPF CVF which constructs a virtual resistor in parallel with the filter capacitor [18]. This method can improve grid side power quality, especially in low frequency region if HPF parameters are properly designed [21]. The MSVF is flexible, robust and

The associate editor coordinating the review of this manuscript and approving it for publication was Elisabetta Tedeschi.

can provide high-bandwidth performance at relatively low switching frequencies [22]. However, the methods of CCF, CVF and MSVF may lead to the insufficient of system PM in the weak grid condition, which will bring out additional stability problem [23]. In addition, extra high precision sensors besides sensors needed by PLL and current/voltage controller are indispensable, which increases system cost greatly [24].

To avoid using extra sensors, [25]–[27] propose a state variable feedback AD method which shares grid-injected current signals with current controller. This method forms a virtual resistor in parallel with the grid-side inductance [26] and a s^2 term appears in the system transfer function, which is usually approximated by a first-order or a high order HPF with a negated output. This type method is also called filter-based AD [27]. Tang *et al.* [28], [17] also propose AD scheme without using extra sensors while using estimation values of needed state variables, such as the capacitor voltage and current. This method is based on high accuracy of system mathematical model [28] and the estimation error will deteriorate system performance or even lead to system instability [17].

Presently, to compensate the PM insufficiency of grid-connected LCL system adopting state variable feedback AD methods such as CCF, CVF and MSVF under the weak grid condition, the lead compensator (LC) has been extensively used in many researches. In [29], [30], and [31], LC is adopted to compensate the robustness problems caused by digital control-delay and presence of grid inductance, etc. However, as discussed previously, extra high sensors are required for signal acquisition. In [32], LC is added in the grid current feedback loop. However, this research adopts first-order HPF connected in series with the LC and the order of the system increases, which makes the parameters design difficult [33].

Control schemes of grid-connected LCL inverter have been investigated extensively and many controllers are developed, such as proportional integral (PI) controller [34], quasi-proportional resonant (QPR) controller [35], deadbeat (DB) controller [36], etc. QPR control can achieve zero steady-state error tracking for periodic signals of a specific frequency (resonant frequency of the QPR controller) due to its infinite gain at the resonant frequency. To improve the adaptability of the LCL inverter to weak grids, many studies are carried out on improved QPR, such as [5], [37].

To improve the robustness and stability of the LCL inverter connected to weak grid, this paper proposes a novel AD. In this scheme, a QPR controller is adopted for the LCL inverter and the grid voltage of common coupling point (v_{pcc}) is feeded back to construct a virtual resistor in parallel with the filter capacitor without extra sensor. Moreover, to increase the PM of the system stability, a LC is presented to approximate s^2 term of system transfer function instead of conventional HPF. Theoretical analysis, simulation and experiment are carried out to verify the effectiveness of the proposed AD scheme.

The structure of this paper is organized as follows: section II presents the mathematical model of the investigated LCL inverter and describes the AD based on v_{pcc} feedback. Section III presents the HPF AD method based on v_{pcc} and detailed procedure of parameter setting is given. Section IV proposes an improved HPF AD, i.e.LC AD, to increase stability phase margin. Section V compares the stability of the HPF AD and the proposed LC AD. Section VI gives the simulation and experimental results and the conclusion is made in section VII.

TABLE 1. System parameters.

Symbol	Description	Value
U_{dc}	DC voltage	180 V
v_g	Grid voltage	100 V
U_{tri}	Amplitude of triangle carrier wave	5.14p.u
L_1	Inverter-side inductance	3 mH
L_2	Grid-side inductance	1 mH
C	Filter capacitance	10 uF
f_0	Grid frequency	frequency50Hz
f_s	Sampling frequency	15 kHZ
f_{sw}	Switching frequency	30 kHZ
I_{ref}	Command current	20A

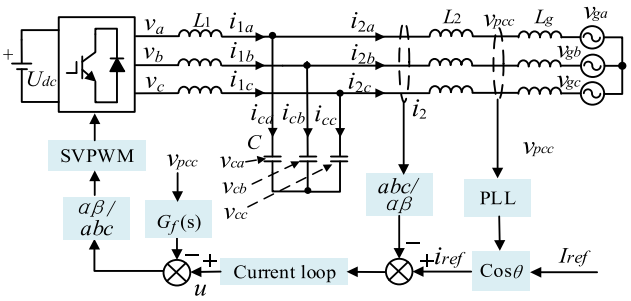

FIGURE 1. Configuration of three-phase LCL grid-connected inverter.

II. SYSTEM DESCRIPTION AND MODELING

A. SYSTEM DESCRIPTION

The configuration of a typical LCL type three-level grid-connected inverter is shown in Fig.1. Where U_{dc} is the DC bus voltage; L_1, L_2 and C_f are the filter inductance and capacitor of LCL filter respectively; v_i and i_{1i} are the output voltages and currents of the inverter ($i = a,b,c$, same below); v_{ci} and i_{ci} are the voltages and currents of C_f; v_{gi} and $i_{2\,i}$ are the grid voltages and grid-injected current; Voltage of common coupling point v_{pcc} is feeded back (VCCPF) and $G_f(s) = 1/K_{PWM}$, K_{PWM} is the inverter gain, which can be expressed as U_{dc}/U_{tri} and U_{tri} is the triangular carrier amplitude [38]. The reference current i_{ref} of grid-injected current is calculated from command I_{ref} which is calculated by upper controller center. The grid impedance is usually composed of the grid resistance R_g and the grid inductance L_g. Because R_g is conducive to the stability of the grid-connected system that it is ignored to carry out following analysis in the worst working conditions. And the parameters of the investigated grid-connected LCL inverter are shown in Table 1.

The mathematical model of the system in frequency domain can be expressed as follows:

$$\begin{cases} sL_1 i_{1i}(s) = v_i(s) - v_{Ci}(s) \\ s(L_2 + L_g) i_{1i}(s) = v_{ci}(s) - v_{gi}(s) \\ sC_f v_{ci}(s) = i_{1i}(s) - i_{2i}(s) \end{cases} \tag{1}$$

Transferring (1) to stationary $\alpha\beta$ reference frame [24], and (2) is obtained:

$$\begin{cases} sL_1 i_{1i\_\alpha\beta}(s) = v_i(s) - v_{ci\_\alpha\beta}(s) \\ s(L_2 + L_g) i_{1i\_\alpha\beta}(s) = v_{ci}(s) - v_{gi\_\alpha\beta}(s) \\ sC_f v_{ci\_\alpha\beta}(s) = i_{1i\_\alpha\beta}(s) - i_{2i\_\alpha\beta}(s) \end{cases} \tag{2}$$

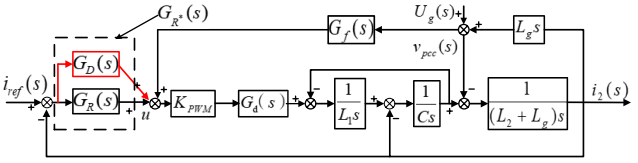

FIGURE 2. Control diagram of grid-connected inverter.

B. CURRENT CONTROL BASED ON QPR

Fig.2 is the control structure diagram of grid-connected inverter shown in Fig.1. To achieve static error free tracking of grid-injected current, a QPR controller is adopted due to its advantages of fast response speed and high robustness and is represented as $G_R(s)$ [22]. Moreover, a multi-resonance compensation controller $G_D(s)$ is in parallel with $G_R(s)$ to suppress the 3rd, 5th, 7th and 9th harmonics of grid voltage [39]. $G_R(s)$, $G_D(s)$ and $G_{R*}(s)$ are as (3):

$$\begin{cases} G_R(s) = K_p + \dfrac{2K_{r1}\omega_c s}{s^2 + 2\omega_c s + \omega_0^2} \\ G_D(s) = \displaystyle\sum_{k=1}^{4} \dfrac{\omega_{fk} s}{s^2 + 2\omega_f s + ((2k+1)\omega_0)^2} \\ G_{R^*}(s) = G_R(s) + G_D(s) \end{cases} \tag{3}$$

where K_p is the overall gain of $G_R(s)$; K_{r1} is the fundamental frequency gain of $G_R(s)$; ω_c is the cut-off frequency of the QPR controller;$\omega_0 = 2\pi f_0$ and f_0 is the fundamental frequency; $2k+1$ represents the harmonic frequency order, $k = 1, 2, 3, 4$; ω_f is the resonance depth; ω_{fk} determines the gain at the harmonic frequency. $G_d(s)$ is the control-delay caused by sampling, A/D and D/A transfer, calculation and PWM modulation and is represented as $e^{-1.5T_s s}$, where T_s is sampling period. Parameters of $G_R(s)$ in (3) are reflected in Table 2 [39], [40].

The open-loop transfer function of the whole system as Fig.2 is:

$$G^1_{i_{ref}-i_2}(s) = G^*_R(s) K_{PWM} G_d(s) / (s^3 L_1 (L_2 + L_g) C + s(L_1 + L_2 + L_g) - L_g s G_d(s)) \tag{4}$$

To simplify analysis, system time delay $G_d(s)$ is ignored (The effects of $G_d(s)$ will be further discussed in section V.)

TABLE 2. Control parameters.

Symbol	Description	Value
K_p	Overall gain	100
K_{r1}	Fundamental frequency gain	0.6
ω_c	Cut-off bandwidth	3.14
ω_f	Depth of the resonance	15
ω_{f1}	3th resonance gain	95
ω_{f2}	5th resonance gain	95
ω_{f3}	7th resonance gain	80
ω_{f4}	9th resonance gain	70

and (4) can be simplified to (5), where $\omega_r = 2\pi f_{ref}$.

$$G^2_{i_{ref}-i_2}(s) = \frac{G_R(s) K_{PWM}}{L_1 C (L_2 + L_g) s} \frac{1}{s^2 + \omega_r^2} \tag{5}$$

According to (5), the resonance frequency f_{ref} of the LCL filer is obtained and shown in (6).

$$f_{ref} = \frac{1}{2\pi} \sqrt{\frac{L_1 + L_2}{L_1 (L_2 + L_g) C}} \tag{6}$$

It is obvious that the open-loop resonant frequency of the system will be affected by L_g inevitably.

C. THE PROPOSED DAMPING SCHEME BASE ON VCCPF

Generally, the power grid with short circuit ratio (SCR) less than 10 is considered as weak grid [41]. In this paper, SCR equals to 10 means L_g is 1mH. According to (5), the Bode diagram can be drawn as Fig.3 and L_g is set to 0.6mH, 1mH, 2mH, 4mH respectively.

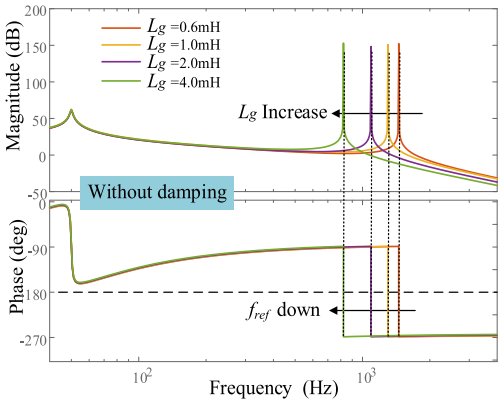

FIGURE 3. Bode diagram of system open-loop control without damping.

Fig.3 clearly shows that the resonance frequency f_{ref} of the grid-connected LCL inverter varies with the change of L_g. Moreover, the phase-frequency characteristic curve crosses the $-180°$ line at the f_{ref}. From a control point of view, this means a pair of closed-loop poles appearing in the right half plane and the system is unstable.

To improve the system stability, a one order damping term, $2\zeta\omega_r s$, is added to (5), and the transfer function

is shown in (7):

$$G^*_{i_{ref}-i_2}(s) = \frac{G_R(s)K_{PWM}}{L_1C(L_2+L_g)s}\frac{1}{s^2+2\zeta\omega_r s+\omega_r^2} \tag{7}$$

To realize the added $2\zeta\omega_r s$ in (7), this paper proposes a v_{pcc} feedback loop and the corresponding transfer function is shown in Fig.4. The proposed AD scheme avoids using extra high precision sensors and is easy for real implementation because the feedback loop is one order system.

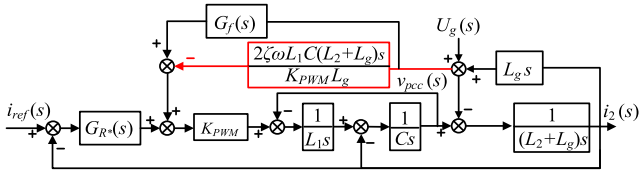

FIGURE 4. Control structure with AD based on v_{pcc} voltage feedback.

III. THE HPF AD BASED ON VCCPF AND PARAMETER SETTING

A. THE HPF AD BASE ON VCCPF

Generally, a HPF is adopted to emulate the added one order system $(2\zeta\omega_1 C(L_2+L_g)s/K_{PWM}L_g)$ in application [42]. (8) is the representation of a one order HPF, where k_h and ω_h are the gain coefficient and cut-off frequency of the HPF.

$$H_{PH}(s) = \frac{k_h s}{s+\omega_h} \tag{8}$$

The system control diagram with a one order HPF is shown in fig.5 and the open-loop transfer function of the system can be obtained as (9), shown at the bottom of the page.

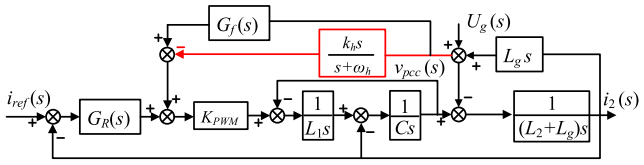

FIGURE 5. Control structure with AD using one order HPF.

B. PARAMETER SETTING OF HPF AD BASED ON VCCPF

In the view of that there is relatively less research on the parameters setting of the AD based on v_{pcc} feedback, this section gives the detailed procedure for parameter setting of HPF AD.

To achieve best damping results, the open transfer function of the whole system should be (10) [25], which means that (9) should be equivalent to (10). Therefore (11) can be obtained:

$$G^*(s) = \frac{G_R(s)K_{PWM}(s+\omega_h)}{L_1(L_2+L_g)Cs(s+m\zeta\omega_m)(s^2+2\zeta\omega_m s+\omega_m^2)} \tag{10}$$

TABLE 3. Robustness comparison.

Cases	PM and GM (L_g=0.6Hm)	PM and GM (L_g=1.0Hm)	PM and GM (L_g=2.0Hm)	PM and GM (L_g=4.0Hm)
m=0.6	41°, 11.0dB	32°, 9.45dB	30°, 7.93dB	21°, 5.52dB
m=1.0	43°, 9.71dB	33°, 8.05dB	30°, 6.62dB	21°, 4.21dB
m=1.4	44°, 9.16dB	35°, 7.56dB	31°, 5.96dB	21°, 3.58dB
m=2.0	43°, 8.51dB	34°, 7.01dB	30°, 5.42dB	19°, 3.04dB
m=3.0	42°, 8.04dB	32°, 6.47dB	28°, 5.14dB	16°, 2.68dB

In (10), ω_m and ζ represent the resonance frequency and damping factor of the conjugate poles. m represents the distance between the real pole and the imaginary axis compared with the distance between conjugate poles and the imaginary axis.

$$\begin{cases} 2\zeta\omega_m + m\zeta\omega_m = \omega_h \\ m\zeta\omega_m^3 = \dfrac{(L_1+L_2)\omega_h}{L_1(L_2+L_g)C} \\ 2m\zeta^2\omega_m^2 + \omega_m^2 = \dfrac{L_1+L_2+K_{PWM}k_hL_g}{L_1(L_2+L_g)C} \end{cases} \tag{11}$$

From the first two equations in (11), the relationship between the m and ω_m can be simplified as:

$$\omega_m = \sqrt{\frac{(m+2)(L_1+L_2)}{mL_1(L_2+L_g)C}} \tag{12}$$

Substituting (12) to the third equation in (11), (13) can be obtained.

$$\begin{cases} K_{PWM}k_h = (\dfrac{m^2+2}{m}+2)\dfrac{(L_1+L_2)}{L_g} \\ \omega_h = \zeta(m+2)\sqrt{\dfrac{(m+2)(L_1+L_2)}{mL_1(L_2+L_g)C}} \end{cases} \tag{13}$$

Assuming $\zeta = 0.707$, the PM and GM (gain margin) of the system with different L_g are shown in Table 3, in which m is set to 0.6, 1, 1.4, 2, 3 and 4 respectively. The corresponding PM curves are shown in Fig.6.

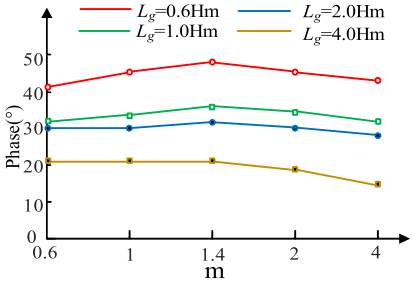

FIGURE 6. PM of different L_g.

As shown in Fig.6, when L_g changes from 0.6mH to 4mH (represented by the value of 0.6mH, 1.0mH, 2.0mH, 4.0mH),

$$G^3_{i_{ref}-i_2}(s) = \frac{G_R(s)K_{PWM}(s+\omega_h)}{(s^4+\omega_h s^3)L_1(L_2+L_g)C + (s^2+\omega_h s)(L_1+L_2) + k_hK_{PWM}s^2L_g} \tag{9}$$

the system has the optimal PM when m is 1.4. Therefore, m is set to 1.4 to achieve high PM in this paper.

Finally, substituting $m = 1.4$ into (13), it can be calculated that $\omega_h = 30625$, $k_h = 19.2$, and these two data will be adopted in following analysis.

IV. LEAD COMPENSATOR AD BASED ON THE IMPROVEMENT OF HPF AD

A. DISADVANTAGES OF THE HPF AD

Under weak grid, the L_g can't be ignored and the stability of LCL inverter will be deeply impacted. According to (9), the open-loop Bode diagram of the system is shown in Fig.7 when L_g changes from 0.6mH to 4mH.

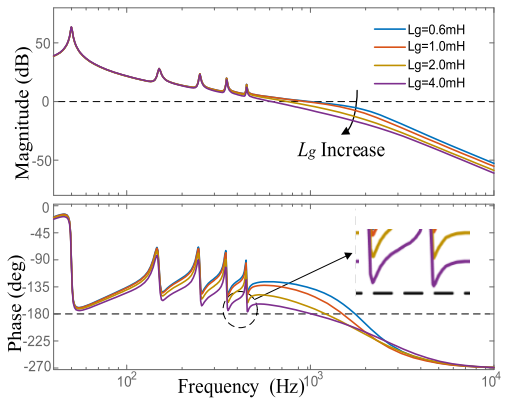

FIGURE 7. Open-loop Bode diagram of different L_g systems with HPF AD.

Fig.7 shows that when the L_g increases, the stability margin of the system decreases and the open-loop cut-off frequency of the system is reduced greatly. For example, when $L_g = 0.6$mH, PM is 43°, f_{cut} is 1152 Hz and the phases of 7th and 9th harmonic are 40° and 36°. However, when $L_g = 4$mH, PM is 15°, f_{cut} is 521 Hz and the phases of 7th and 9th harmonic are only 10° and 7°. Considering the influence of control delay, the open-loop PM of the system may be further reduced, and the resonance peak will intersect the −180° line, which means that harmonics around cross point will be amplified and the power quality of system will be deteriorated.

B. THE PROPOSED LC AD

In order to compensate PM of the LCL inverter with HPF AD based on VCCPF in the weak grid condition, a LC AD is proposed in this paper as shown in Fig.8 and the transfer function $H_{LC}(s)$ is shown in (14). Comparing to H_{PF}(s) shown in (8), a constant k_c is adopted to compensate the system PM. The open-loop transfer function of the system is expressed as (15).

$$H_{LC}(s) = \frac{k_h s + k_c}{s + \omega_h} \tag{14}$$

$$G^*_{I_{ref}-I_2}(s) = \omega_m = G_R(s)K_{PWM}(s+\omega_h)/((L_2+L_g)C + (s^2+\omega_h s)(L_1+L_2) + (k_h s^2 + k_c s)K_{PWM}L_g) \tag{15}$$

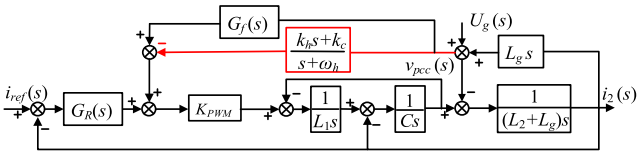

FIGURE 8. Transfer function diagram of the system with HPF AD.

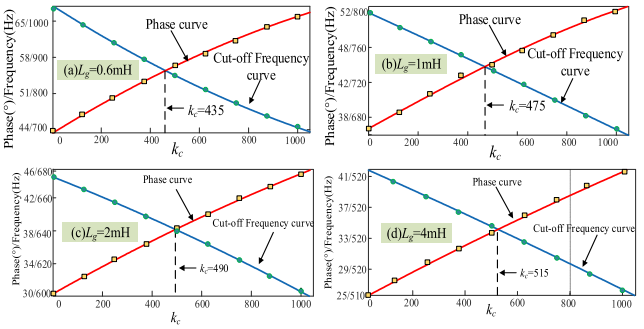

FIGURE 9. System phase and cutoff frequency vs. k_c.

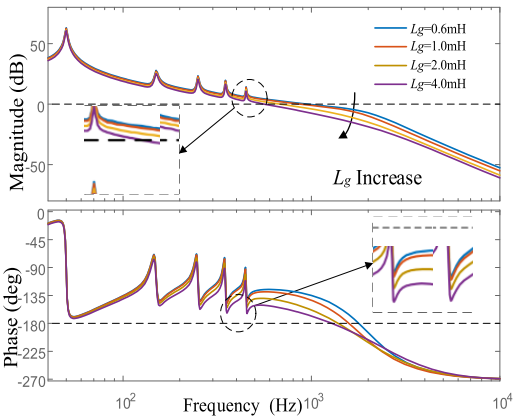

FIGURE 10. Open-loop Bode diagram of the system with LC AD under different L_g.

Fig. 9 shows the relationship of the system phase and cut-off frequency versus k_c of different L_g condition, which is obtained by fitting curve method under Matlab and k_c changes in the range of (0, 1000). Obviously, when k_c increases, the phase margin of the system increases while the open-loop cut-off frequency decreases. Fig.9 also shows that at the cross points, k_c equals to 435, 475, 490 and 515, respectively. Therefore, to ensure the open-loop system has a combined good performance of phase margin and cutoff frequency when the L_g varies, the intermediate value $k_c = 475$ is selected in this paper.

The Bode diagram according to (15) is shown in Fig.10, where grid impedance L_g is set to 0.6mH to 4mH to represent different weak grid situations. Comparing Fig.7 and Fig.11, it can be concluded that with the proposed LC AD, the system PM is improved greatly (for example, when $L_g = 4$mH, PM is 15° with HPF AD and is 36° with LC AD). Typically, the crossing of the −180° line appearing in HPF AD when $L_g = 4$mH is disappeared, which means that LC AD is

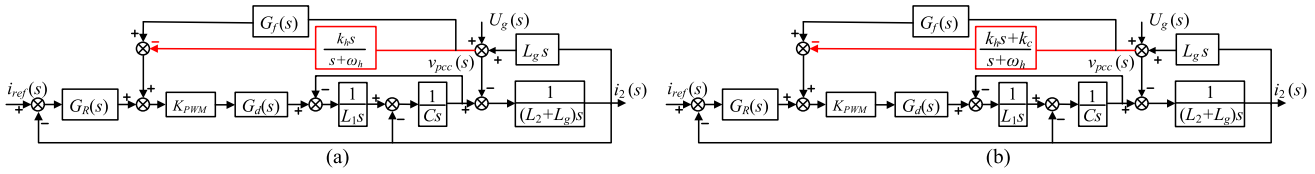

FIGURE 11. Control diagrams of the system (a) HPF AD, (b) LC AD.

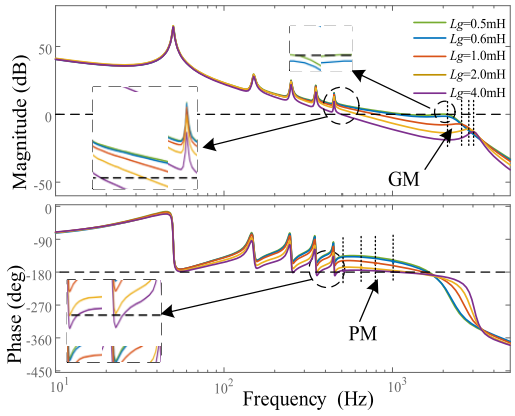

FIGURE 12. The open-loop Bode plot of the system with HPF AD.

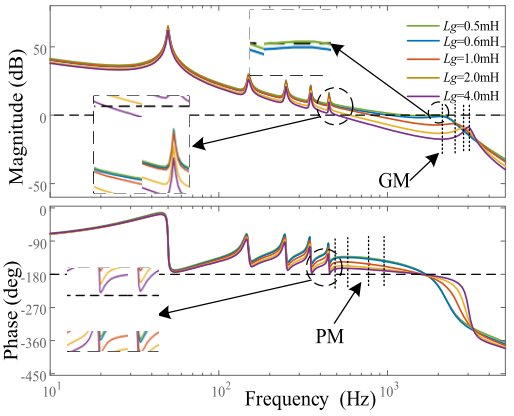

FIGURE 13. The open-loop Bode plot of the system with LC AD.

conducive to improve system stability in addition to provide system damping.

V. SYSTEM STABILITY ANALYSIS

When considering system time delay, the control diagrams of the investigate LCL inverter system are as Fig.11 in which $G_d(s)$ is system time delay and its Pade expression is represented by (16) [18]. The open loop transfer functions of the system with HPF AD and proposed LC AD are shown as (17) and (18), at the bottom of the page, respectively, and corresponding Bode diagrams are shown in Fig.12 and Fig.13.

$$G_d(s) = e^{-1.5T_s s} \approx \frac{1 - \frac{T_d s}{2} + \frac{(T_d s)^2}{12}}{1 + \frac{T_d s}{2} + \frac{(T_d s)^2}{12}} \tag{16}$$

It should be noted that comparing to Fig 7 and 10, which ignore the influence of $G_d(s)$, Fig.12 and Fig.13 show that the presence of $G_d(s)$ will decrease PM.

Fig.12 shows that when L_g increases from 0.6mH to 4mH with HPF AD, GM increases from 3.3dB to 15.6 dB and PM decreases from 39° to 2° (f_{cut} decreases from 1021Hz to 518Hz). Taking 7th and 9th harmonic as examples, when L_g equals to 2mH, the phases are very close to −180°, and as L_g grows more higher, the phase may below 180°(such as when L_g equals to 4mH, the phase has less than −180°).

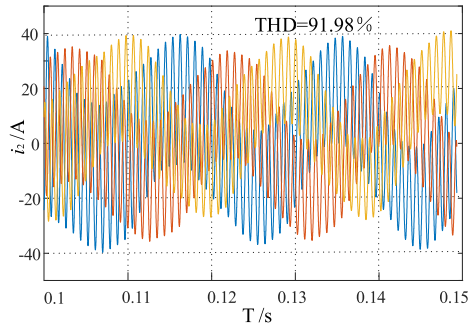

FIGURE 14. i_2 without AD when L_g is 4mH.

Fig.13 shows that with the proposed LC AD strategy, when L_g increases from 0.6mH to 4mH, the GM increases from 2.1dB to 15.8 dB and the PM decreases from 41° to 16° (f_{cut} decreases from 950Hz to 492Hz). Fig.13 also shows that the −180° line acrossing of 7th and 9th harmonics (at 350Hz and 450Hz) in Fig.12 is disappeared.

Since most of the power grids in remote mountainous areas of Sichuan Province, China are in the weak grid state (SCR less than 10), this paper proposes an active damping method based on the grid voltage based on this. And in this article, when SCR = 10, the corresponding L_g is 1mH. And stability range of HPF AD is only (0.6mH, 2mH), and the proposed

$$G^{PF}_{I_{ref}-I_2}(s) = \frac{G_R(s)K_{PWM}(s+\omega_h)G_d(s)}{(s^4+\omega_h s^3)L_1(L_2+L_g)C + (s^2+\omega_h s)(L_1+L_2+L_g-L_g G_d(s)) + k_h s^2 K_{PWM} G_d(s) L_g} \tag{17}$$

$$G^{LC}_{I_{ref}-I_2}(s) = \frac{G_R(s)K_{PWM}(s+\omega_h)G_d(s)}{(s^4+\omega_h s^3)L_1(L_2+L_g)C + (s^2+\omega_h s)(L_1+L_2+L_g-L_g G_d(s)) + (k_h s^2+k_c s)K_{PWM} G_d(s) L_g} \tag{18}$$

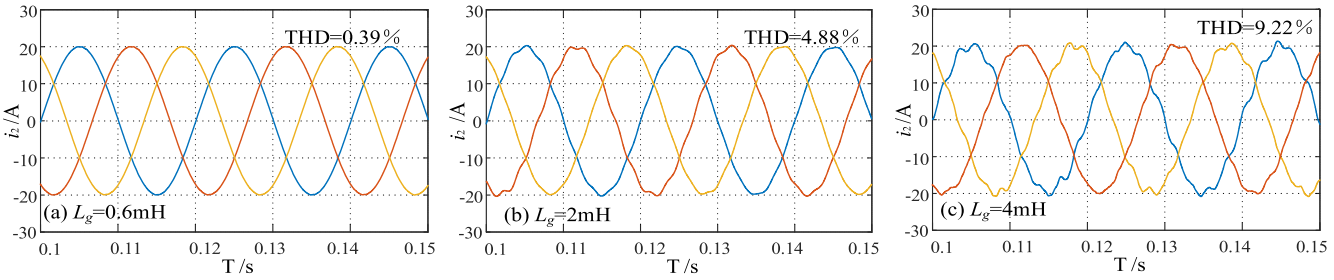

FIGURE 15. i_2 with HPF AD under different L_g.

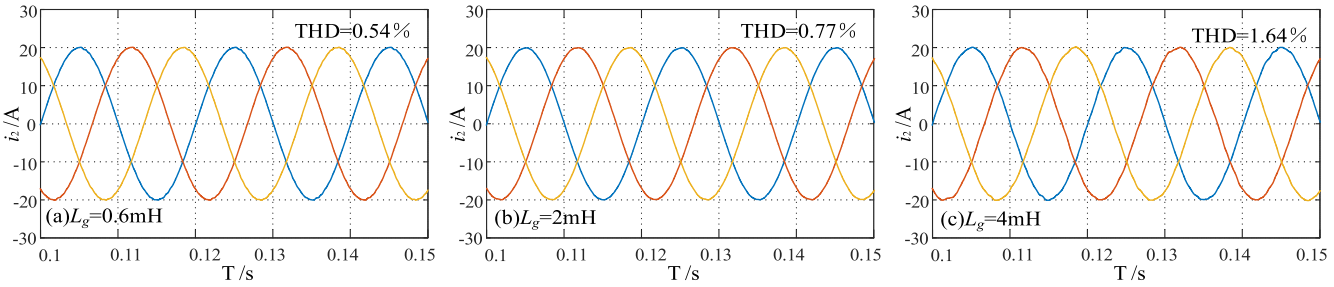

FIGURE 16. i_2 with LC AD under different L_g.

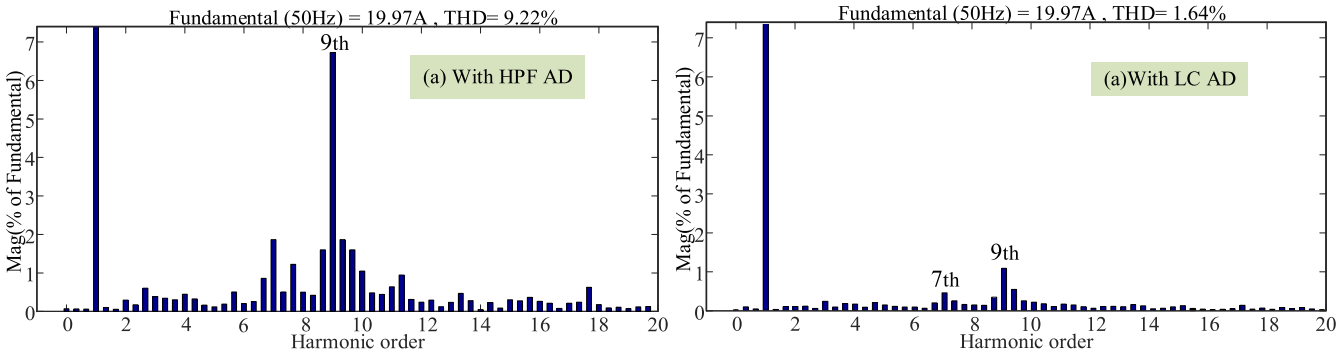

FIGURE 17. FFT analysis of the i_2 under distorted grid voltage when L_g is 4mH. (a) HPF AD, (b) LC AD.

LC AD increases the stability range of the system to (0.6mH, 4mH).

It should be noted that, the grid is named as weak grid if SCR is larger than 1 (corresponding to L_g is larger than 1mH in this paper). Therefore, even considering the variation of L_g, the minimum value of 0.6mH is sufficient to demonstrate the effectiveness of aboved HPF AD and LC AD

VI. SIMULATION AND EXPERIMENT

A. SIMULATIONS

A simulation based on MATLAB/SIMULINK for the LCL inverter as shown in Fig.1 is carried out and parameters used are shown in Table 1 and Table 2. In the simulation, two aspects of system performance are investigated: (1) effectiveness of HPF AD and LC AD. (2) dynamic performance test of the two methods. 3th, 5th, 7th and 9th harmonics are injected into grid voltage to simulate real grid voltage harmonics and corresponding magnitudes are 0.1, 0.05, 0.03, 0.02 respectively [43]. Simulation results of grid-injected currents i_2 are as Fig.14-Fig.16, Fig.17 is Fast Fourier Transform (FFT) analysis of i_2 when $L_g = 4$mH.

Fig.14 shows that the system cannot keep stable without AD. Fig.15(a) and Fig.16(a) show that when L_g is 0.6mH, both HPF AD and LC AD can keep the system stable, which is consistent with the theoretical analysis. Fig.15(b) shows that with HPF AD, the waveform of i_2 appears distortion and total harmonic distortion (THD) reaches 4.88% while with LC AD, THD is only 1.64%. Similarly, as shown in Fig.15(c) and Fig.16(c), when $L_g = 4$mH, the current waveform using the HPF AD is severely distorted, and the THD is as high as 9.22%. As analysis before, it is because the phase of 7th and 9th are lower than 180° which causes the 7th and 9th harmonics to be severely amplified, as shown in Fig.17(a). But when the LC AD is adopted, the THD of the i_2 reduces to 1.64%, as shown in Fig.17(b). Thus, it is concluded that system with LC AD has better stable performance than HPF AD when L_g varies in a wide range, which makes the LC AD suitable for weak grid condition.

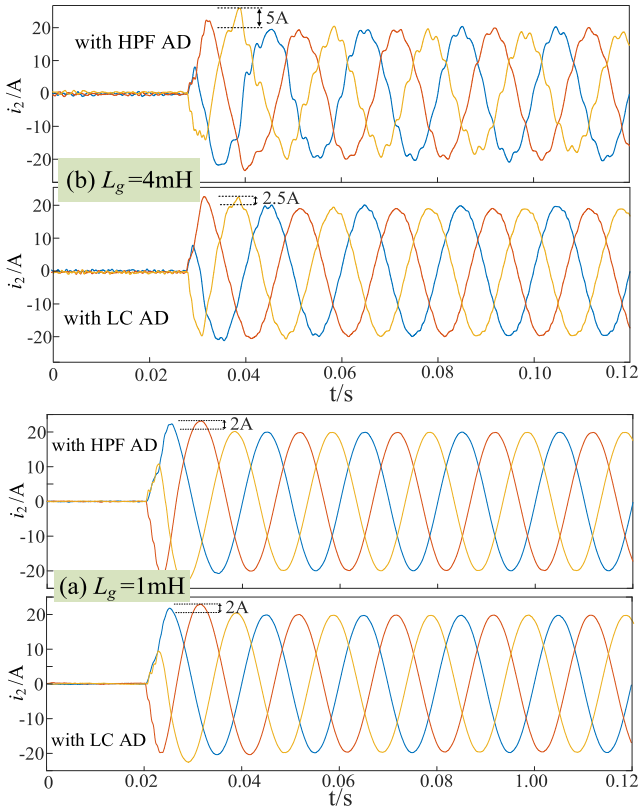

FIGURE 18. i_2 when reference signal mutation.

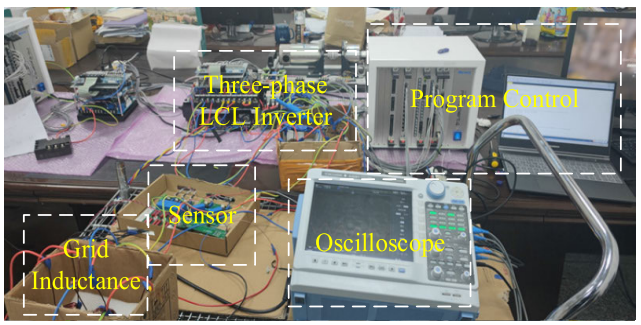

FIGURE 19. Three-phase LCL type grid-connected inverter experiment platform.

Fig.18 shows the dynamic response of the system jump from 0 to 20A with HPF AD and LC AD respectively, where L_g is 1mH and 4mH respectively. The grid current reference signal i_{ref} is set to jump from 0A to 20A. It can be seen that with the large jump of the command, when $L_g = 1$mH, both the HPF AD and LC AD can track the reference signal accurately and the overshoot current are 2A. When L_g increases to 4mH, the dynamic performance of system with HPF AD is poor and the current overshoot reaches 5A. However, when LC AD is applied to the system with same L_g, the system dynamic performance is improved and the current overshoot is only 2.5A.

B. EXPERIMENTS

In order to verify the aforementioned HPF AD and LC AD on the experimental platform, transfer functions in (3)(8)(14)

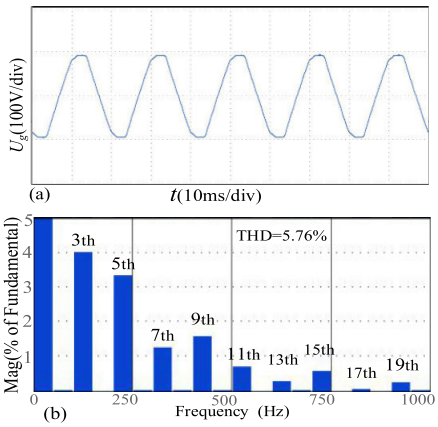

FIGURE 20. The waveform of the U_g and its FFT analysis.

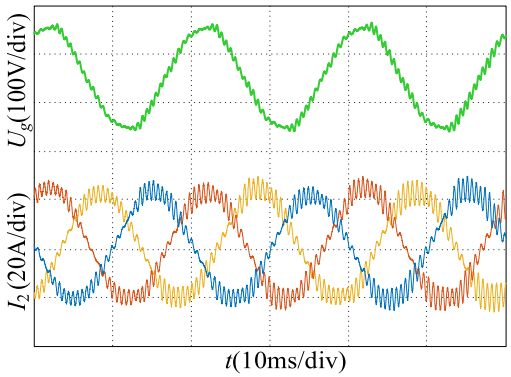

FIGURE 21. Grid-injected current i_2 without AD when L_g is 4mH.

TABLE 4. Main component specifications.

Project	Specification
Current sensor	HAS50-S (50A/4V)
Voltage sensor	CVC-25 (500V/5V)
Electrolytic capacitor	ERWE451LGC152MCB5M (1500 μ F/450V)
IGBT-IPM	7MBP50RJ120
Diode module	PT5221
Electromagnetic relay	SD-N35(CX) DC24V
Digital signal processor	TMS320C6657
Switching power supply	FBA100F-24 (DC24 4.5A)
Relay	SSR-3D4830A

should be discretized. The method of Tustin [30] is used to discretize the control part. According to the discretization method of Tustin, the discretization expression of (3) can be derived as (19), shown at the bottom of the next page, and the discretization expression of (8) can be derived as (20), shown at the bottom of the next page, where $T_s \approx 0.05$ms is the control period, and $A = (2m + 1)^2$. It is worth noting that assigning K_c in $H_{LC}(z)$ to 0 can obtain the discretization formula of $H_{PF}(z)$.

Fig.19 is the experimental platform, in which a 9.1 kW three-phase LCL inverter is connected to grid. The DC side of the inverter is supplied with an adjustable transformer and a rectifier. The output side of the LCL inverter is connected

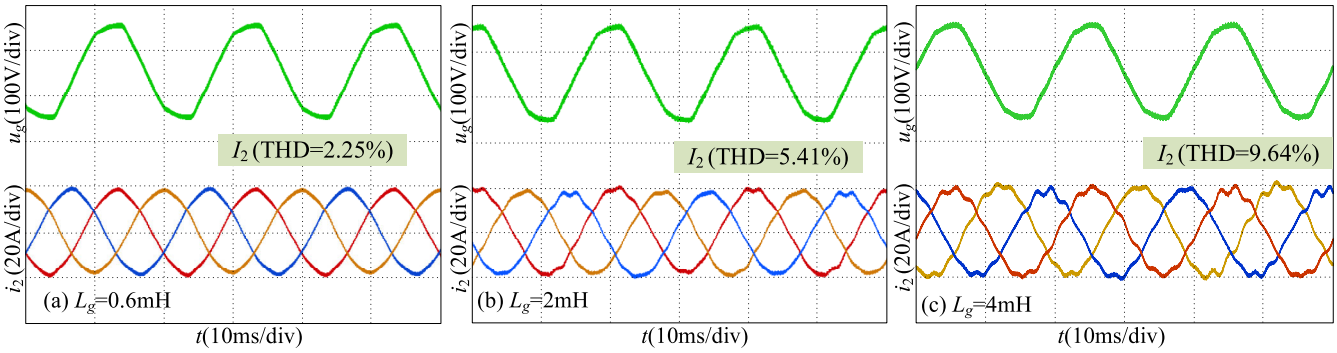

FIGURE 22. Grid-injected current i_2 when HPF AD is applied.

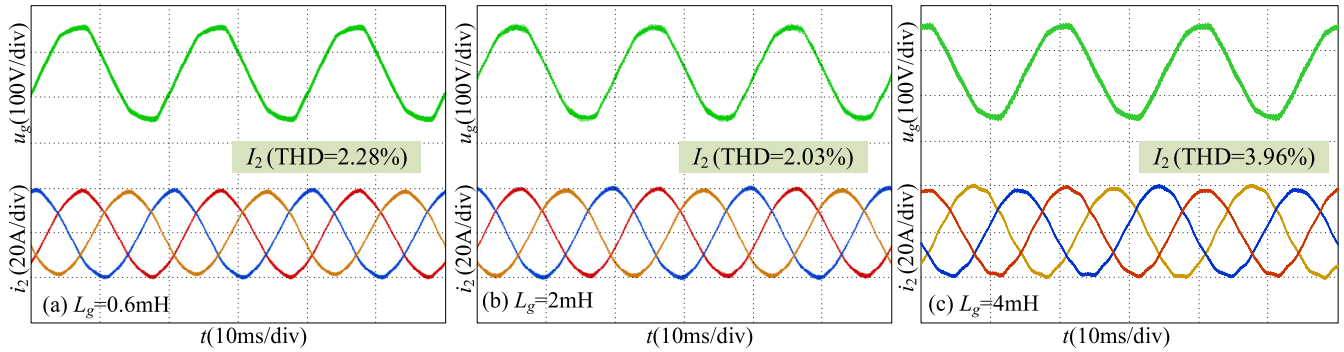

FIGURE 23. Grid-injected current i_2 when LC AD is applied.

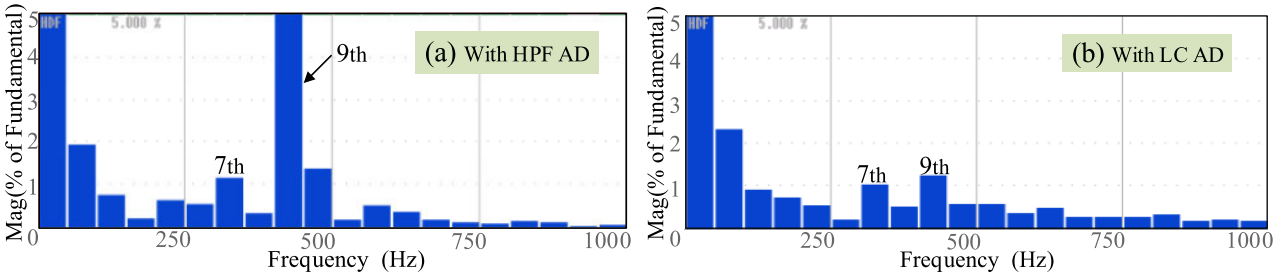

FIGURE 24. FFT analysis of the i_2 under distorted grid voltage when L_g is 4mH. (a) HPF AD, (b) LC AD.

to the grid through a relay. Parameters of the components used in the experimental platform are shown in Table 1 and Table 2. Moreover, the experimental hardware model is shown in Table 4.

Fig. 20(a) shows the grid voltage u_g measured in the lab and it contains 3th, 5th, 7th and 9th harmonic voltages as the FFT analysis in Fig.20(b).

Fig.21 shows that without AD method, i_2 has a large harmonic oscillation which means the system is unstable. Fig.22(a) shows with HPF AD, when $L_g = 0.6$mH, the grid-injected current i_2 has relatively ideal waveform and the THD is only 2.25%. When L_g is 2mH, i_2 has a slight distortion and the THD increases to 5.41%, which is shown in Fig.22(b). This is because the reduced PM causes the phase of resonance

$$G_R^*(z) = K_p + \frac{K_{r1}\omega_c T(z^2-1)}{(\omega_c T + \frac{1}{4}T^2\omega^2 + 2)z^2 + (\frac{1}{2}T^2\omega^2 - 2)z + (1 - \omega_c T + \frac{1}{4}T^2\omega^2)} + \sum_{m=1}^{3} \frac{\omega_{fm} T(z^2-1)}{(2\omega_f T + \frac{1}{2}AT^2\omega^2)z^2 + (AT^2\omega^2 - 4)z + (2 - 2\omega_f T + \frac{1}{2}AT^2\omega^2)} \tag{19}$$

$$H_{LC}(z) = \frac{(k_h + k_c)z - (k_c - k_h)}{(0.5T\omega_h + 1)z + (0.5T\omega_h - 1)} \tag{20}$$

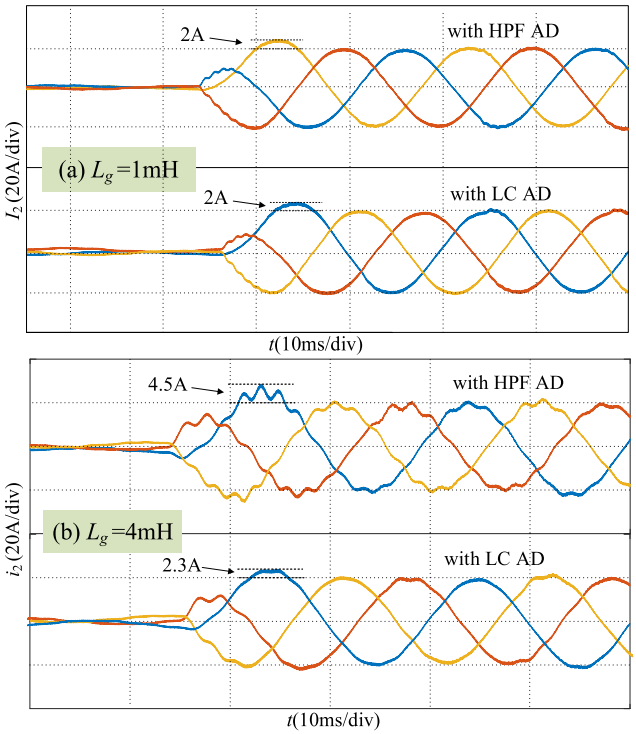

FIGURE 25. Experimental transient waveforms of the reference steps down when L_g is 1mH and 4mH.

peak to approach the −180° line. Fig.22(c) shows that when L_g increases to 4mH, the PM of the system is already seriously insufficient in the frequency of 350Hz and 450Hz, especially, the 9th harmonic in the i_2 is amplified greatly, and the THD increases to 9.64% according to Fig.24(a). This means that when L_g increases, the stability performance of LCL inverter system with HPF AD becomes worse, which is consistent with results of theoretical analysis and simulation.

Fig.23 (a), (b) and (c) are the experimental waveforms of i_2 with LC AD. It can be seen that i_2 maintains little distortion when L_g increases from 0.6 to 4mH, and the THD of i_2 are 2.28%, 2.03% and 3.96%, which are much lower than that when the HPF AD is applied.

Finally, the dynamic responses of the LCL inverter system with HPF AD and LC AD are compared by experiments. Fig.25 shows the dynamic process of i_2 when $L_g = 1$mH and 4mH and i_{ref} jumps from 0A to 20A. In coincidence with the simulation results, system with HPF AD and LC AD both have better dynamic response when $L_g = 1$mH, and the overshoot current are 2A. But when $L_g = 4$mH, the overshoot current of HPF AD increases to 4.5A, while with LC AD it is only 2.3A. It means that the proposed LC AD can improve the dynamic performance of LCL inverter more effectively, especially under a large L_g.

VII. CONCLUSION

To improve power quality and stability of weak grid-connected LCL filter inverter with QPR controller, a new active damping scheme, LC AD, is proposed to increase system PM, which avoids using extra high-precision sensors. Detailed theory analysis, parameters setting are given in the paper. Simulation and experiment results show that comparing with the traditional HPF AD, the LC AD can provide better damping effect and can improve system stability more effectively, which makes it especially suitable for LCL inverter under weak grid condition to achieve high robustness and dynamic response.

It is worth noting that this LC AD is developed specially for weak grid situation. If the grid impedance is too small or even absent, the effect of the proposed LC AD will be deteriorated. This problem can be resolved by the method of LC combined with other AD methods using single-loop control, such as grid injection current feedback, etc.

REFERENCES

[1] F. Blaabjerg, R. Teodorescu, M. Liserre, and A. V. Timbus, "Overview of control and grid synchronization for distributed power generation systems," *IEEE Trans. Ind. Electron.*, vol. 53, no. 5, pp. 1398–1409, Oct. 2006.

[2] R. Peña-Alzola, M. Liserre, F. Blaabjerg, R. Sebastián, J. Dannehl, and F. W. Fuchs, "Analysis of the passive damping losses in LCL-filter-based grid converters," *IEEE Trans. Power Electron.*, vol. 28, no. 6, pp. 2642–2646, Jun. 2013.

[3] P. A. Daly and J. Morrison, "Understanding the potential benefits of distributed generation on power delivery systems," in *Proc. IEEE Rural Electr. Power Conf.*, Little Rock, AR, USA, Apr./Feb. 2001, pp. 1–13.

[4] Y. Han, M. Yang, H. Li, P. Yang, L. Xu, E. A. A. Coelho, and J. M. Guerrero, "Modeling and stability analysis of LCL-type grid-connected inverters: A comprehensive overview," *IEEE Access*, vol. 7, pp. 114975–115001, 2019.

[5] M. Su, B. Cheng, Y. Sun, Z. Tang, B. Guo, Y. Yang, F. Blaabjerg, and H. Wang, "Single-sensor control of LCL-filtered grid-connected inverters," *IEEE Access*, vol. 7, pp. 38481–38494, 2019.

[6] J. Xu and S. Xie, "LCL-resonance damping strategies for grid-connected inverters with LCL filters: A comprehensive review," *J. Mod. Power Syst. Clean Energy*, vol. 6, no. 2, pp. 292–305, Mar. 2018.

[7] K. Jalili and S. Bernet, "Design of LCL filters of active-front-end two level voltage-source converters," *IEEE Trans. Ind. Electron.*, vol. 56, no. 5, pp. 1674–1689, May 2009.

[8] X. Li and H. Lin, "A design method of phase-locked loop for grid-connected converters considering the influence of current loops in weak grid," *IEEE J. Emerg. Sel. Topics Power Electron.*, vol. 8, no. 3, pp. 2420–2429, Sep. 2020.

[9] W. Zhao and G. Chen, "Comparison of active and passive damping methods for application in high power active power filter with LCL-filter," in *Proc. Int. Conf. Sustain. Power Gener. Supply*, Nanjing, China, Apr. 2009, pp. 1–6.

[10] S. Eren, M. Pahlevaninezhad, A. Bakhshai, and P. K. Jain, "Composite nonlinear feedback control and stability analysis of a grid-connected voltage source inverter with LCL filter," *IEEE Trans. Ind. Electron.*, vol. 60, no. 11, pp. 5059–5074, Nov. 2013.

[11] J. Dannehl, M. Liserre, and F. W. Fuchs, "Filter-based active damping of voltage source converters with LCL filter," *IEEE Trans. Ind. Electron.*, vol. 58, no. 8, pp. 3623–3633, Aug. 2011.

[12] R. Peña-Alzola, M. Liserre, F. Blaabjerg, M. Ordonez, and T. Kerekes, "A self-commissioning notch filter for active damping in a three-phase LCL-filter-based grid-tie converter," *IEEE Trans. Power Electron.*, vol. 29, no. 12, pp. 6754–6761, Dec. 2014.

[13] W. Yao, Y. Yang, X. Zhang, F. Blaabjerg, and P. C. Loh, "Design and analysis of robust active damping for LCL filters using digital notch filters," *IEEE Trans. Power Electron.*, vol. 32, no. 3, pp. 2360–2375, Mar. 2017.

[14] E. Twining and D. G. Holmes, "Grid current regulation of a three-phase voltage source inverter with an LCL input filter," *IEEE Trans. Power Electron.*, vol. 18, no. 3, pp. 888–895, May 2003.

[15] G. Shen, X. Zhu, J. Zhang, and D. Xu, "A new feedback method for PR current control of LCL-filter-based grid-connected inverter," *IEEE Trans. Ind. Electron.*, vol. 57, no. 6, pp. 2033–2041, Jun. 2010.

[16] D. Pan, X. Ruan, C. Bao, W. Li, and X. Wang, "Capacitor-current-feedback active damping with reduced computation delay for improving robustness of LCL-type grid-connected inverter," *IEEE Trans. Power Electron.*, vol. 29, no. 7, pp. 3414–3427, Jul. 2014.

[17] J. Dannehl, F. W. Fuchs, and P. B. Thøgersen, "PI state space current control of grid-connected PWM converters with LCL filters," *IEEE Trans. Power Electron.*, vol. 25, no. 9, pp. 2320–2330, Sep. 2010.

[18] X. Zhou and S. Lu, "A novel inverter-side current control method of LCL-filtered inverters based on high-pass-filtered capacitor voltage feedforward," *IEEE Access*, vol. 8, pp. 16528–16538, 2020.

[19] J. Xu, S. Bian, Q. Qian, H. Qian, and S. Xie, "Robustness improvement of single-phase inverters under weak grid cases by adding grid current feedforward in delay-based phase-locked loop," *IEEE Access*, vol. 8, pp. 124275–124287, 2020.

[20] E. Wu and P. W. Lehn, "Digital current control of a voltage source converter with active damping of LCL resonance," *IEEE Trans. Power Electron.*, vol. 21, no. 5, pp. 1364–1373, Sep. 2006.

[21] Z. Xin, P. C. Loh, X. Wang, F. Blaabjerg, and Y. Tang, "Highly accurate derivatives for LCL-filtered grid converter with capacitor voltage active damping," *IEEE Trans. Power Electron.*, vol. 31, no. 5, pp. 3612–3625, May 2016.

[22] B. Shu, M. Gao, D. Zhang, K. Meng, R. N. Ashraf, and Y. Wang, "Control strategy of three-phase inverter under weak grid condition," in *Proc. Int. Conf. Smart Grids Energy Syst. (SGES)*, Nov. 2020, pp. 740–745.

[23] Z. Miao, W. Yao, and Z. Lu, "Single-cycle-lag compensator-based active damping for digitally controlled LCL/LLCL-type grid-connected inverters," *IEEE Trans. Ind. Electron.*, vol. 67, no. 3, pp. 1980–1990, Mar. 2020.

[24] X. Chen, Y. Zhang, S. Wang, J. Chen, and C. Gong, "Impedance-phased dynamic control method for grid-connected inverters in a weak grid," *IEEE Trans. Power Electron.*, vol. 32, no. 1, pp. 274–283, Jan. 2017.

[25] J. Xu, S. Xie, and T. Tang, "Active damping-based control for grid-connected LCL-filtered inverter with injected grid current feedback only," *IEEE Trans. Ind. Electron.*, vol. 61, no. 9, pp. 4746–4758, Sep. 2014.

[26] X. Wang, F. Blaabjerg, and P. C. Loh, "Grid-current-feedback active damping for LCL resonance in grid-connected voltage-source converters," *IEEE Trans. Power Electron.*, vol. 31, no. 1, pp. 213–223, Jan. 2016.

[27] M. Buyuk, A. Tan, M. Inci, and M. Tumay, "A notch filter based active damping of llcl filter in shunt active power filter," in *Proc. Int. Symp. Power Electron. (Ee)*, Oct. 2017, pp. 1–6.

[28] Y. Tang, P. C. Loh, P. Wang, F. H. Choo, and F. Gao, "Exploring inherent damping characteristic of LCL-filters for three-phase grid-connected voltage source inverters," *IEEE Trans. Power Electron.*, vol. 27, no. 3, pp. 1433–1443, Mar. 2012.

[29] T. Fang, S. Shen, L. Zhang, Y. Jin, and C. Huang, "Capacitor-current-feedback with phase-lead compensator to eliminate resonant frequency forbidden region for LCL-type grid-connected inverter in weak grid," *IEEE J. Emerg. Sel. Topics Power Electron.*, early access, Feb. 12, 2021, doi: 10.1109/JESTPE.2021.3059024.

[30] F. Bronchart, Y. Mollet, and J. Gyselinck, "LCL filters for a grid emulator application–comparative study of active damping techniques," in *Proc. 39th Annu. Conf. IEEE Ind. Electron. Soc. (IECON)*, Nov. 2013, pp. 2087–2092.

[31] M. T. Faiz, M. M. Khan, X. Jianming, S. Habib, and H. Tang, "Parallel feedforward compensation based active damping of LCL-type grid connected inverter," in *Proc. IEEE Int. Conf. Ind. Technol. (ICIT)*, Feb. 2018, pp. 788–793.

[32] L. Zhou, X. Zhou, Y. Chen, Z. Lv, Z. He, W. Wu, L. Yang, K. Yan, A. Luo, and J. M. Guerrero, "Inverter-current-feedback resonance-suppression method for LCL-type DG system to reduce resonance-frequency offset and grid-inductance effect," *IEEE Trans. Ind. Electron.*, vol. 65, no. 9, pp. 7036–7048, Sep. 2018.

[33] X. Wan, X. Ding, and H. Hu, "An improved active damping method based on single-loop inverter current control for LCL resonance in grid-connected inverters," *Math. Problems Eng.*, vol. 2021, pp. 1–11, Mar. 2021.

[34] J. Dannehl, C. Wessels, and F. W. Fuchs, "Limitations of voltage-oriented PI current control of grid-connected PWM rectifiers with LCL filters," *IEEE Trans. Ind. Electron.*, vol. 56, no. 2, pp. 380–388, Feb. 2009.

[35] C. Bao, X. Ruan, X. Wang, W. Li, D. Pan, and K. Weng, "Step-by-step controller design for LCL-type grid-connected inverter with capacitor–current-feedback active-damping," *IEEE Trans. Power Electron.*, vol. 29, no. 3, pp. 1239–1253, Mar. 2014.

[36] J. Hu, "Improved dead-beat predictive DPC strategy of grid-connected DC–AC converters with switching loss minimization and delay compensations," *IEEE Trans. Ind. Informat.*, vol. 9, no. 2, pp. 728–738, May 2013.

[37] Q. An, J. Zhang, Q. An, and A. Shamekov, "Quasi-proportional-resonant controller based adaptive position observer for sensorless control of PMSM drives under low carrier ratio," *IEEE Trans. Ind. Electron.*, vol. 67, no. 4, pp. 2564–2573, Apr. 2020.

[38] Y. Guan, Y. Wang, Y. Xie, Y. Liang, A. Lin, and X. Wang, "The dual-current control strategy of grid-connected inverter with LCL filter," *IEEE Trans. Power Electron.*, vol. 34, no. 6, pp. 5940–5952, Jun. 2019.

[39] Y. Fan, L. Jun, and L. Bingbing, "Study of current control strategy of STATCOM based on LCL filter under distorted grid conditions," in *Proc. China Int. Conf. Electr. Distrib. (CICED)*, Xi'an, China, Aug. 2016, pp. 1–5.

[40] L. A. Lucas, M. A. G. Brito, and R. C. Garcia, "A photovoltaic multifunctional converter with multi-resonant controller coefficients improved by a genetic algorithm," in *Proc. IEEE 27th Int. Conf. Electron., Electr. Eng. Comput. (INTERCON)*, Aug. 2019, pp. 1–4.

[41] A. Etxegarai, P. Eguia, E. Torres, and E. Fernandez, "Impact of wind power in isolated power systems," in *Proc. 16th IEEE Medit. Electrotech. Conf.*, Mar. 2012, pp. 63–66.

[42] M. Hanif, V. Khadkikar, W. Xiao, and J. L. Kirtley, "Two degrees of freedom active damping technique for LCL filter-based grid connected PV systems," *IEEE Trans. Ind. Electron.*, vol. 61, no. 6, pp. 2795–2803, Jun. 2014.

[43] X. Huang, Z. Gao, C. Yang, and F. Liu, "State estimation of continuous-time linear fractional-order systems disturbed by correlated colored noises via Tustin generating function," *IEEE Access*, vol. 8, pp. 18362–18373, 2020.